SPE-173222-MS

Geomechanics Coupling Simulation of Fracture Closure and Its Influence on Gas Production in Shale Gas Reservoirs

Cong Wang, Yu-Shu Wu, Yi Xiong, and Philip H. Winterfeld, Colorado School of Mines; Zhaoqin Huang, China University of Petroleum (East China)

This paper was prepared for presentation at the SPE Reservoir Simulation Symposium held in Houston, Texas, USA, 23–25 February 2015.

Abstract

A sharp initial decline in the production rate is being experienced in many shale gas plays. One reason is the closure of natural micron and micro fractures. The natural fractures, which widely exist in the over-pressurized source rock, react sensitively to the change of subsurface stress. The change in stress can be caused by the decrease of gas pressure during production. These fracture closure or re-open phenomena have significant effects on reservoir permeability and gas production.

In this paper, a fully coupled geomechanics and multiphase fluid flow model is presented to accurately simulate the fields of stress and fluid flow in shale gas reservoirs. Several relationships between fracture closure and applied stress are incorporated in this model, based on the experimental data from literatures. Therefore, the stress dependency of shale natural fractures is quantified and modeled in its full complexity. The natural fractures in this model are characterized as stiff, self-propped, and prone to closure. It represents an extension of our earlier "hybrid-fracture model" (DFN for hydraulic fractures, double-porosity for natural fractured domain inside the SRV, and single porosity or dual-continuum outside the SRV).

Introduction

Shale formation is characterized by extraordinarily low permeability and existence of various scaled natural fractures. Previous experimental and numerical studies prove that the economical production in these reservoirs is difficult to achieve without the contribution of some natural fractures. This is because matrix permeability of these rocks is extremely low, typically ranging from nanodarcy to microdarcy. Gas flow velocity just through this tight matrix is almost zero based on Darcy's law (Wang et al. 2013; Xiong et al. 2014).

Natural fractures in these reservoirs are generated from tectonic activities and thermal maturity processes of hydrocarbon. In the thermal maturity process, kerogen in these shale formations was transformed into bitumen, and then became oil and gas. It was a hydrocarbon volume increasing process. The final volume of the gas could be 10 times more than the original volume of kerogen. Most of these generated gases were not free to immigrate. They were trapped where they were generated from, because the source rock was so tight (Apaydin, 2012). The pressure inside the pores therefore keptto increase

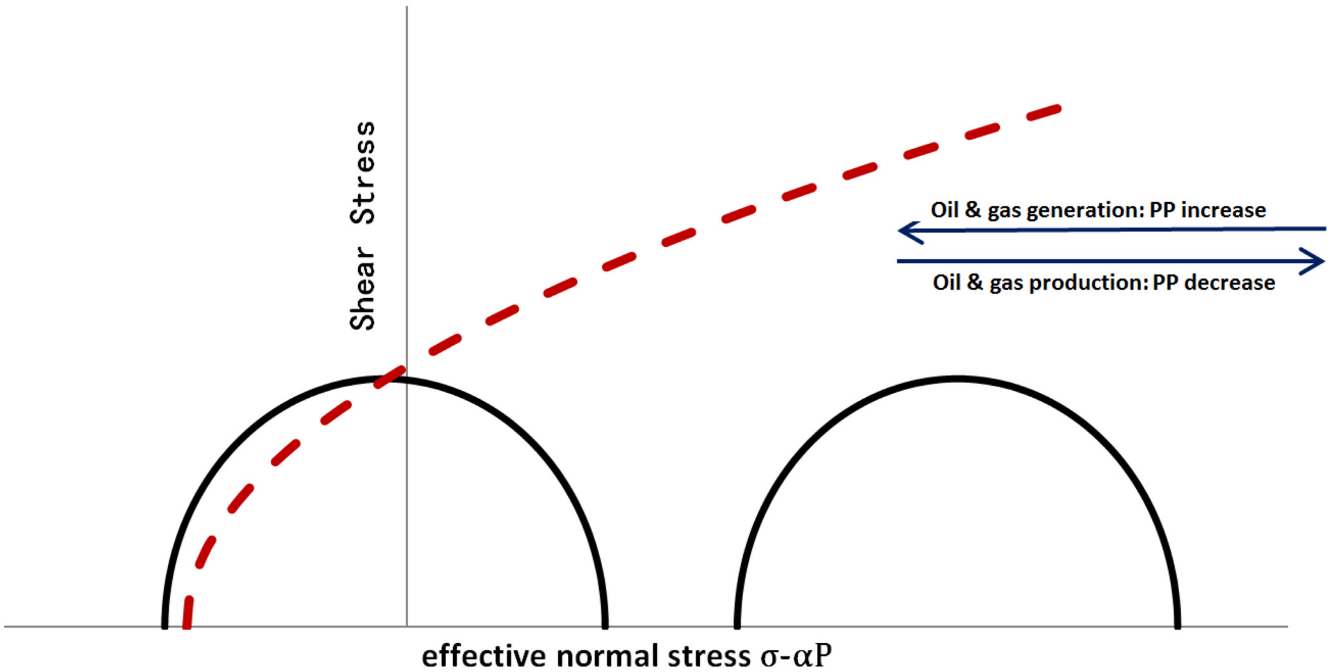

Figure 1—Mohr's circle move with hydrocarbon generation and production

correspondingly. Fractures were opened where the local pressure exceeded the combination of minimum stress and tensile strength. The occurrence of fractured reservoirs is observed to be in close association with over-pressure regions in the unconventional plays.

Figure 1 presents standard graphical Mohr's circle and failure envelope. If the point of tangency between the stress circle and failure envelope is on positive or compressive side of the coordinates, the rocks will fail in the form of shear form. If the tangency is on negative or tensile side of the origin, the fracture will be in the form of open extension (Meissner, 1978). The hydrocarbon generation process discussed above will move the stress circle to the left, which generates the set of tensile fractures. While the hydrocarbon production moves the circle back to the right, these tensile fractures close again.

A rather sharp initial decline in the production rate is experienced in these shale plays when compared with conventional reservoirs. Recent perspectives provide the basis for blaming the closure of these generated tensile natural fractures for this decline behavior. The natural fractures, which widely exist in the over-pressured source rock, react very sensitively to the change of critical stresses due to gas production. Their closure and re-open have quite large effects on gas flow or production.

In conventional reservoirs, effect of geomechanics on rock deformation and permeability is generally small and has been ignored mostly in practice. In unconventional shale formations, however, such geomechanics effect can be large and has a significant impact, especially, on properties of fractures, which has to be considered in general. Study (Soeder, 1988; Wang et al. 2009) shows that permeability in the Marcellus Shale is pressure dependent and decreases with an increase in confining pore pressure (or total stress). The effect of confining pressure on permeability is caused by a reduction of pore volume or porosity. Bustin et al. (2008) report the effect of stress (confining pressure) in Barnett, Muskwa, Ohio, and Woodford shales. The degree of permeability reduction with confining pressure is significantly higher in shale than in consolidated sandstone or carbonate. Another example of geomechanics effect shows an estimate of the effect of closure stress on unpropped-fracture conductivity in Marcellus shale for a Young's modulus of 2 MMpsi, based on previously published work (Cipolla et al. 2009) and revised on the basis of Barnett shale history-matching results. The initial network-fracture conductivity is 2 md-ft before production, but declines to 0.02 md-ft, when the pressure in the network fractures decreases to the FBHP of 500 psi.

In this paper, a fully coupled geomechanics and fluid flow model is presented to accurately simulate the field of stress and fluid flow in shale gas reservoirs. We provide a comprehensive description of the mathematical formulation and numerical method for fluid flow and geomechanics in multi-porosity medium. Empirical relationships between fracture closure and applied stress are incorporated based on the literature, where testing was completed under laboratory conditions. Therefore the stress dependency of shale natural fractures is quantified and modeled in its full complexity. The natural fractures in this model are characterized as stiff, self-propped, and prone to closure. It represents an extension of our earlier "hybrid-fracture model" (DFN for the hydraulic fractures, MINC for natural fractured area inside SRV and single porosity for the area outside SRV) that did not account for dynamics of fracture properties.

Fluid Flow Governing Equations

The two phase flow model, gas and water (or liquid), in a porous or fractured unconventional reservoir is assumed to be similar with what is described in the black oil model. It is composed only of two phases: gaseous and aqueous phases. For simplicity, the gas and water components are assumed to be present only in their associated phases and adsorbed gas is within the solid phase of rock. Each phase flows in response to pressure, gravitational, and capillary forces according to the multiphase extension of Darcy law or several extended non-Darcy flow laws, discussed below. In an isothermal system containing two mass components, subject to multiphase flow and adsorption, two mass-balance equations are needed to fully describe the system, as described in an arbitrary flow region of a porous or fractured domain for flow of phase β (β = g for gas and β= w for water),

$$\frac{\partial}{\partial t}\left(\Phi S_\beta \rho_\beta + m_g\right) = -\nabla \cdot \left(\rho_\beta v_\beta\right) + q_\beta \tag{1}$$

where Φ is the effective porosity of porous or fractured media; S_β is the saturation of fluid β; ρ_β is the density of fluid β; v_β is the volumetric velocity vector of fluid β, determined by Darcy's law or non-Darcy's flow models, discussed in the below; t is time; m_g is the adsorption or desorption mass term for gas component per unit volume of rock formation; and q_β is the sink/source mass term of phase (component) β per unit volume of formation.

Geomechanical Equations

The geomechanical equations in fluid-saturated porous media are based on "mean-stress" model. Several inherent assumptions for the development of the geomechanics module are listed as follows:

- Rock mechanics properties are isotropic
- Rock behaves as a perfectly elastic media (linear, reversible and non-retarded mechanical behavior)
- Rock deformation are relatively small and can be accurately computed using small strains assumption;

The classical theory of elasticity extended to multi-porosity media. In a double-porosity medium consisting of a network of fractures and rock matrix, the stress-strain behavior of an elastic material is described by Hooke's law:

$$\bar{\bar{\sigma}} - \left(\sum_j \alpha_j P_j\right)\bar{I} = 2G\bar{\epsilon} + \lambda\left(tr\bar{\epsilon}\right)\bar{I} \tag{2}$$

Where σ is the stress tensor; subscript j refers to a multi-porosity continuum such as fracture or matrix; α is the Biot coefficient and has the different values for the fracture and matrix medium; P is pore pressure; G is shear modulus; λ is the Lamé parameter; $\bar{\bar{\epsilon}}$ is the strain tensor, and I is the identity matrix.

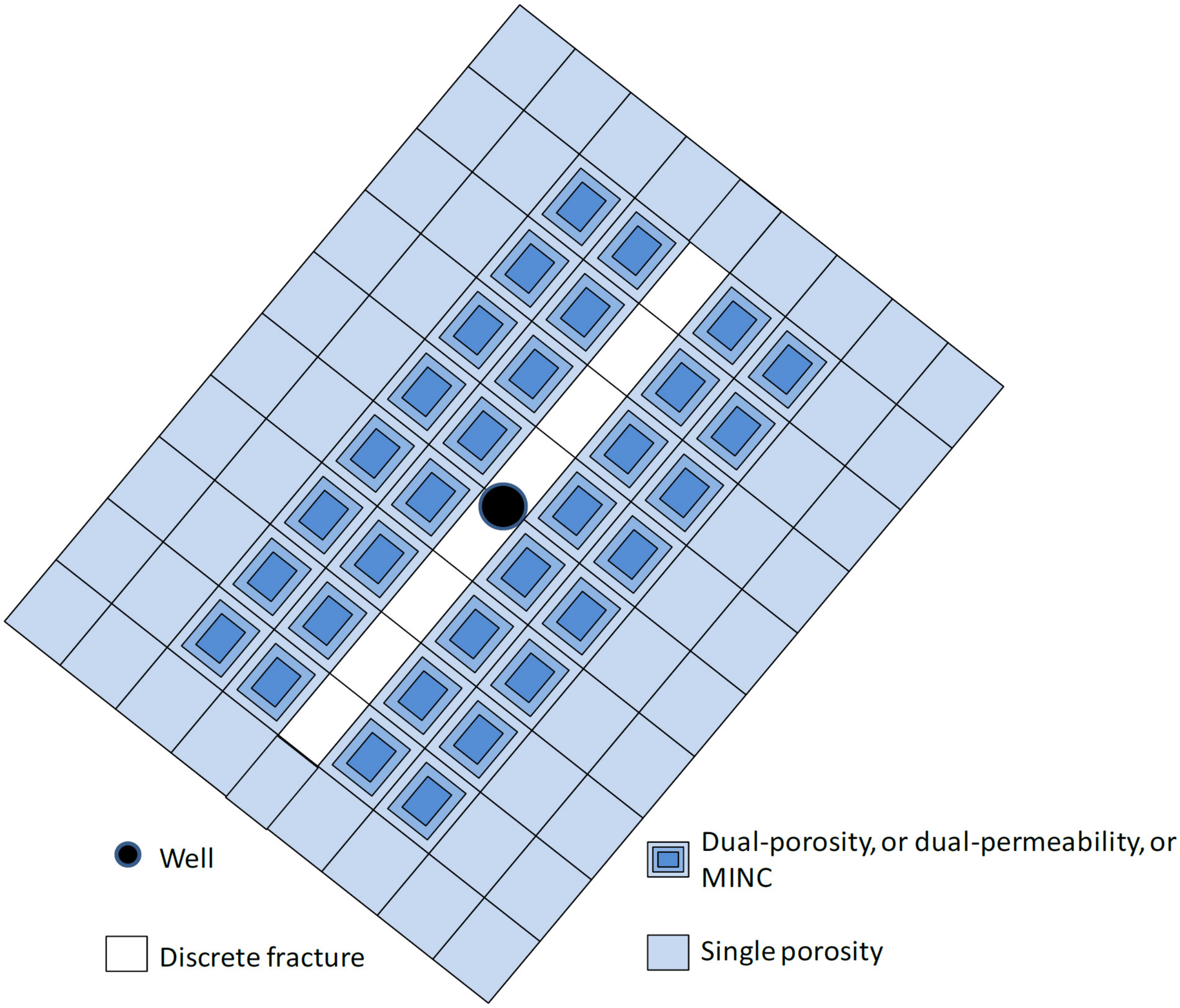

Figure 2—Sketch of the hybrid fracture model

The relation between strain tensor and the displacement vector, $\bar{u}$:

$$\bar{\bar{\epsilon}} = \frac{1}{2}(\nabla\bar{u} + \nabla\bar{u}^t) \tag{3}$$

And the static equilibrium equation:

$$\nabla \cdot \bar{\bar{\sigma}} + \bar{F}_b = 0 \tag{4}$$

where $\bar{F}_b$ is the body force. We combine the above three equations to obtain the multi-porosity elastic Navier equation for the isothermal system:

$$\nabla\left(\sum_j \alpha_j P_j\right) + (\lambda + G)\nabla(\nabla \cdot \bar{u}) + G\nabla^2\bar{u} + \bar{F}_b = 0 \tag{5}$$

Take the divergence of the above equation,

$$\nabla^2\left(\sum_j \alpha_j P_j\right) + (\lambda + 2G)\nabla^2(\nabla \cdot \bar{u}) + \nabla \cdot \bar{F}_b = 0 \tag{6}$$

The divergence of the displacement vector is the sum of the normal strain components, the volumetric strain:

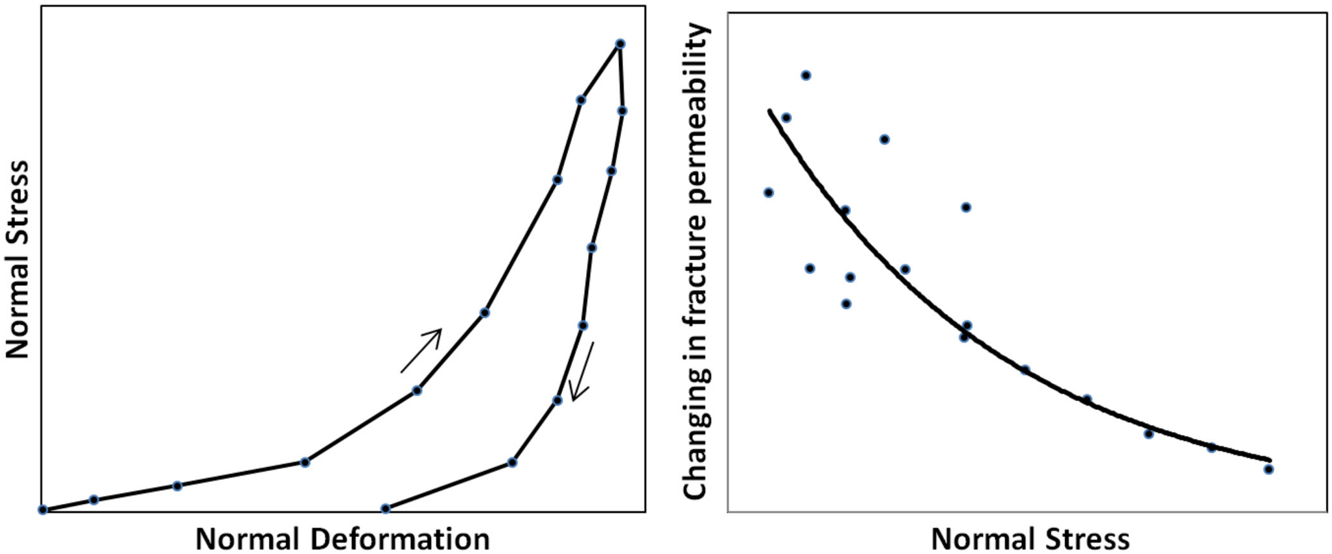

Figure 3—Empirical correlations between normal stress and normal deformation, between fracture permeability and normal stress

$$\nabla \cdot \bar{u} = \frac{\partial u_x}{\partial x} + \frac{\partial u_y}{\partial y} + \frac{\partial u_z}{\partial z} = \epsilon_{xx} + \epsilon_{yy} + \epsilon_{zz} = \epsilon_v \tag{7}$$

Combining these equations yields an equation relating mean stress, pore pressure, and body force:

$$K\epsilon_v = \sigma_m - \sum_j \alpha_j P_j \tag{8}$$

$$\nabla \cdot \left[\frac{3(1-v)}{1+v} \nabla \sigma_m + \bar{F}_b - \frac{2(1-2v)}{1+v} \nabla \left(\sum_j \alpha_j P_j\right)\right] = 0 \tag{9}$$

Equations (8) and (9) are the governing geomechanical equations and mean stress and volumetric strain are the geomechanical variables associated with those equations. Equation (9) is a statement of momentum conservation in terms of mean stress and other variables and Equation (8) is a property relation, relating volumetric strain to mean stress and other variables (Jaeger, et al. 2009; Winterfeld and Wu, 2014; Xiong et al. 2013).

Stress-sensitive Hybrid Fracture Model

The hybrid-fracture modeling approach, defined as a combination of explicit-fracture (discrete fracture model), double-porosity, and single-porosity modeling approaches, seems to be the best option for modeling a shale gas reservoir with both hydraulic fractures and natural fractures (Wu and Wang, 2014; Wu and Fakcharoenphol, 2011). This is because hydraulic fractures, which have to be dealt with for shale gas production, are better handled by the explicit fracture method, and they cannot be modeled in general by a dual-continuum model. On the other hand, natural fractured reservoirs are better modeled by a dual-continuum approach, such as double-porosity or MINC model for extremely low-permeability matrix and long lasting transient flow in shale gas formations, which cannot be modeled by an explicit fracture or classic double-porosity model (Figure 2).

In a stress-sensitive hybrid fracture model, permeability and porosity of the fracture system are sensitive to the effective stress, while the properties of the matrix system are relatively insensitive. Some experiment data indicate that the fracture conductivity exhibits a decline of 2 orders of magnitude with the increase of stress from 2,000psi to 6,000psi and this reduction is permanent. The permeability of propped fractures (hydraulic fracture in this model) also declines with the increase of effective stress, but not as severe as in the unpropped fractures (Miller et al. 2010).

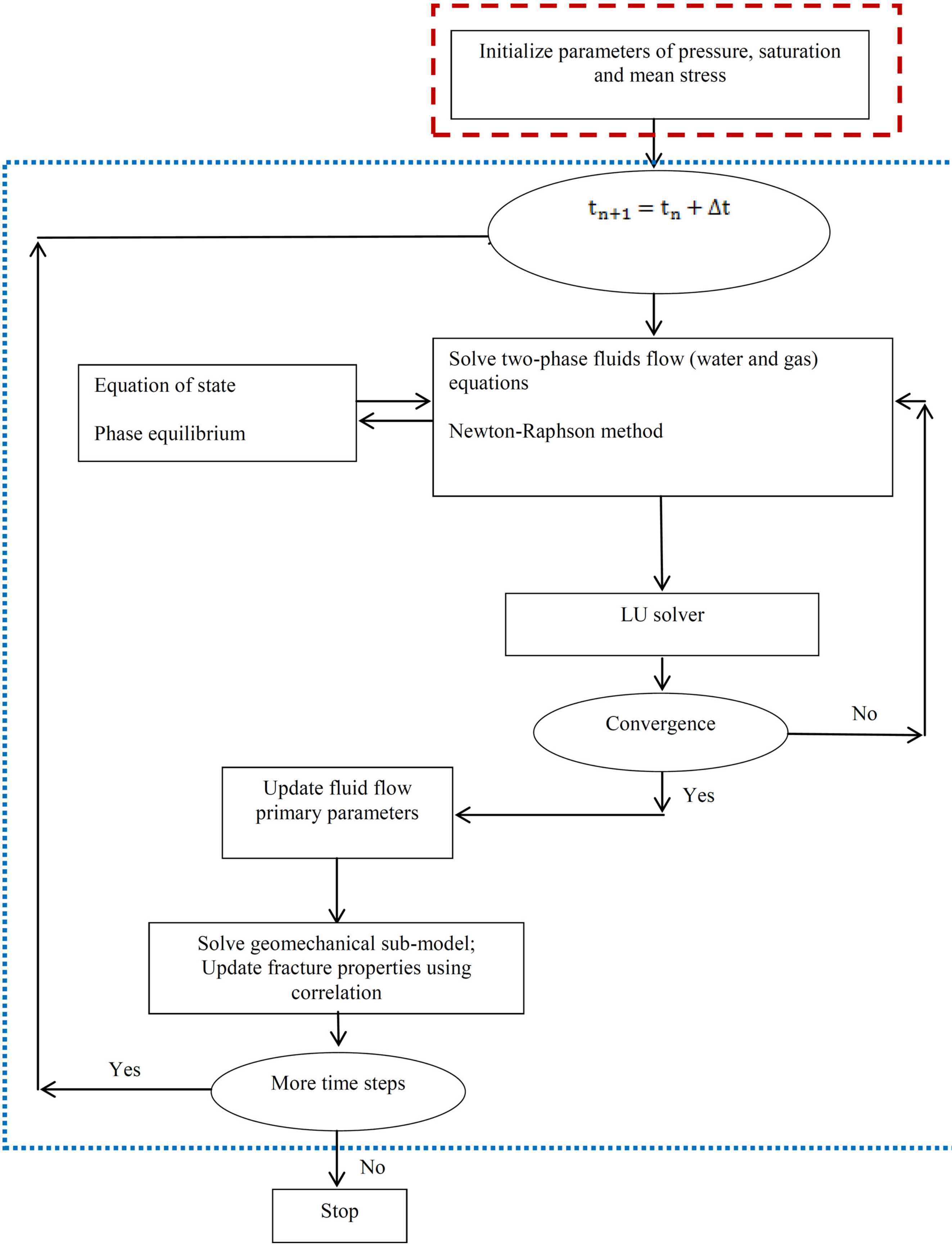

Figure 4—Model structure for loose-coupling fluids flow, geomechanics, and fracture properties correlation

The permeability-stress relationship of the fractured rocks has been investigated by many researchers (Gutierrez, 2000;Baghbanan and Jing, 2008; Zhang et al. 2007). Typically increasing the normal stress reduces the fracture opening and increases the contact area. With the increasing contact area, the fracture becomes stiffer and makes itself more difficult to close with the increasing normal stress. However, these fractures never completely close and their permeability are always larger than the shale matrix permeability; even the normal stress is higher than the unconfined compressive strength of the intact shale.

A hypothetical correlation curve is shown in the Figure 3 (Gutierrez, 2000). The exponential dependence of permeability on normal stress is commonly observed in a fractured medium, so we use the following relationship between permeability and normal stress:

$$k = k_0 e^{-C\sigma_n'} \tag{10}$$

Where k_0 is the average of the initial permeability; σ_n' is effective normal stress along the fractures, and C is is an empirical constant which is also an average for the samples.

Some other correlations between effective stress and rock properties are reported by researchers. Rutqvist et al. (2002) present the following function for porosity, obtained from laboratory experiments on sedimentary rock (Davies and Davies, 1999),

$$\Phi = \Phi_r - (\Phi_0 - \Phi_r)e^{-a\sigma'} \tag{11}$$

where Φ_0 is zero effective stress porosity; Φ_r is high effective stress porosity, and the exponent a is a parameter. They also present an associated function for permeability in terms of porosity,

$$k = k_0 e^{-c\left(\frac{\Phi}{\Phi_0}-1\right)} \tag{12}$$

where c is a parameter.

Ostensen (1986) studies the relationship between effective stress and permeability for tight gas sands and approximated permeability as

$$k^n = D ln \frac{\sigma'^*}{\sigma} \tag{13}$$

where exponential n is 0.5; D is a parameter; and σ'^* is effective stress for zero permeability, obtained by extrapolating permeability versus effective stress on a semi-log plot.

Numerical implementation

We developed two coupling approaches, loose coupling and fully coupling, to combine the fluids flow module and geomechanics module. The second approach is coupled on each iteration level therefore it provides a more accurate simulation of the subsurface stress and fluid conditions (Settari and Walters, 2001; Settari, 2002). However, a much larger Jacobian matrix is required to build in this approach, which increases the calculation cost a lot. From the perspective of model application, most of the reservoirs are deeply located. Their stress condition is high and stable. The change of pressure with production is relatively small in terms of this large stress. Then the loose coupling approach is accurate enough for these cases. In unconventional reservoirs, however, the subsurface stress condition is unstable after hydraulic fracturing. The hydraulic fractures and fracking-induced natural fractures are also very sensitive to this unstable subsurface stress. Special cares need to be taken in reservoir simulation to capture this process accurately especially in the early phase of production (Wu and Wang, 2014).

Figure 4 is the illustration of loose coupling method. The key procedure to incorporate the geomechanics effect for this approach is:

1. Calculate effective stress or their change at the end of each time step as functions of pressure
2. Calculate porosity, permeability of the fractures as functions of mean stress

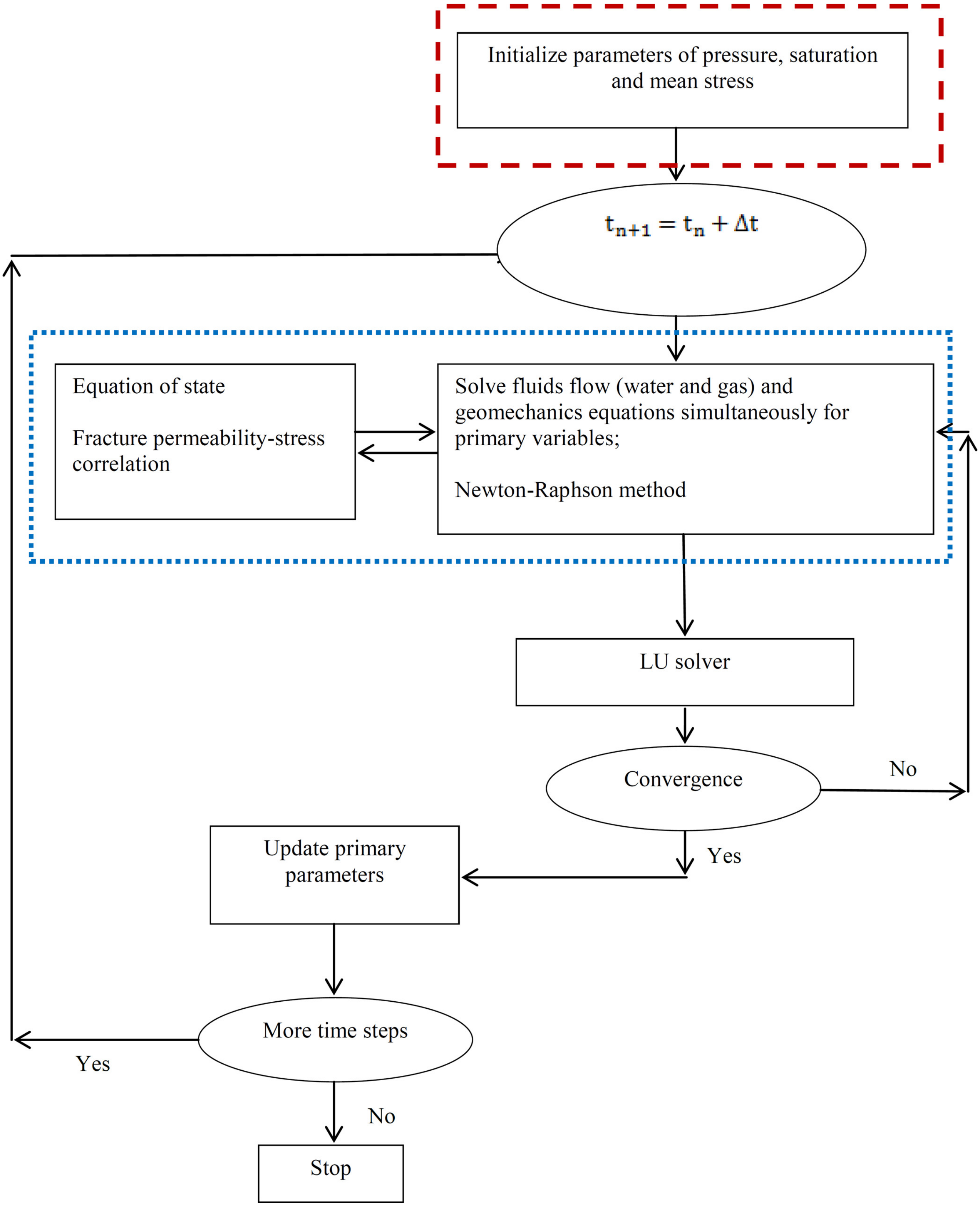

Figure 5—Model structure for fully-coupling fluids flow, geomechanics, and fracture properties correlation

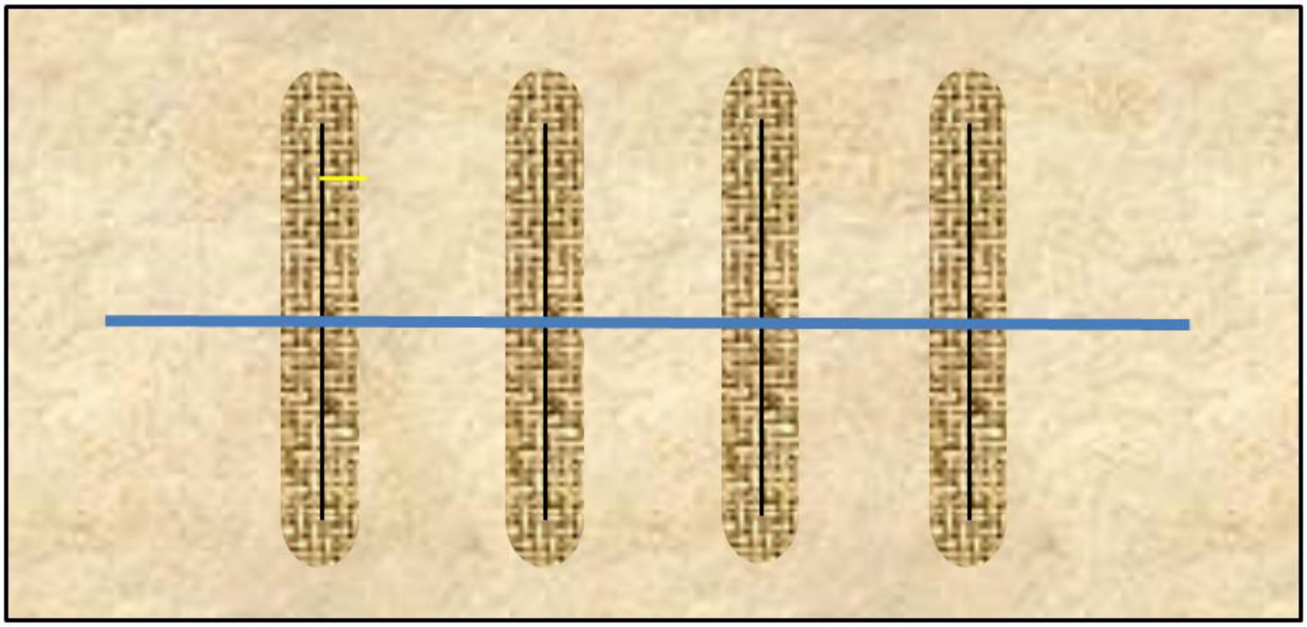

Figure 6—Horizontal well, multi-stage hydraulic fracture, and SRV model

3. Substitute the modified porosity and permeability values in calculation of the accumulation term and flow term for the next time calculation.

Figure 5 illustrates the flow chart for solving the full-coupled process of multiphase fluid flow and geomechanics in a multi-porosity medium. In this numerical model, the mass, energy and momentum conservation equations are solved simultaneously. Note that in this fully coupled flow-mechanics calculation, these calculations are done at Newton-Raphson iteration level, not time-step level. They are discretized in space by the integral finite difference method (Pruess et at. 1999). Time discretization is carried out using a backward, first-order, fully implicit finite-difference scheme. The model solves three primary variables (pressure, gas saturation, and mean stress) for each grid block. The primary variables, pressure and gas saturation, are solved from the mass conservation Equation (1). Mean stress is from Equation (9). These equations are solved by the Newton-Raphson iteration method, and the Jocobian matrix coefficients are calculated by the numerical approach.

The set of coupled nonlinear mass and energy conservation equations can be written in residual form as:

$$R_i^{\beta,n+1} = M_i^{\beta,n+1} - M_i^{\beta,n} - \frac{\Delta t}{V}\left(\sum_j A_{ij} F_{ij}^{\beta} + V_i q_i^{\beta,n+1}\right) = 0 \tag{14}$$

Similar to the mass and energy equations, the finite difference approximation for the geomechanics equation in residual form is:

$$R_i^{\beta,n+1} = \sum_j \left[\frac{3(1-\nu)}{1+\nu}\frac{\sigma_{mj}-\sigma_{mi}}{d_{ij}} - \frac{2\alpha(1-2\nu)}{1+\nu}\frac{p_j-p_i}{d_{ij}} + \boldsymbol{f}\cdot\boldsymbol{n}\right]_{ij} A_{ij} = 0 \tag{15}$$

The initial pressure, saturation, and stress fields are predetermined as a function of spatial coordinates. The key procedure to incorporate the geomechanics effect is:

1. Solve the mean stress with pressure and saturation together.
2. Calculate effective stress or their change at each Newtonian iteration as functions of pressure and mean stress
3. Calculate porosity, permeability of the fractures as functions of mean stress

Table 1—Input formation parameters for the simulation

Reservoir depth, h, ft	5800	Hydraulic fracture porosity, Φ_{hf}	0.5
Formation thickness, Δz, ft	328	Young's Modulus, E, GPa	5.0
Matrix porosity, Φ_m	0.05	Poisson's ratio, γ	0.25
Matrix permeability, k_m, md	3.2E-05	Biot's coefficient, α	1.0
Hydraulic fracture half-length, X_f, ft	290	Hydraulic fracture half-height, h_f, ft	30
Gas viscosity, μ, cp	0.0184	Natural Fracture Spacing, m	10
Distance between hydraulic fractures, $2y_e$, ft	200	Constant flowing bottomhole pressure, P_{wf}, psi	1000
Initial reservoir pressure, P_i, psi	3800	Hydraulic fracture stages number	20

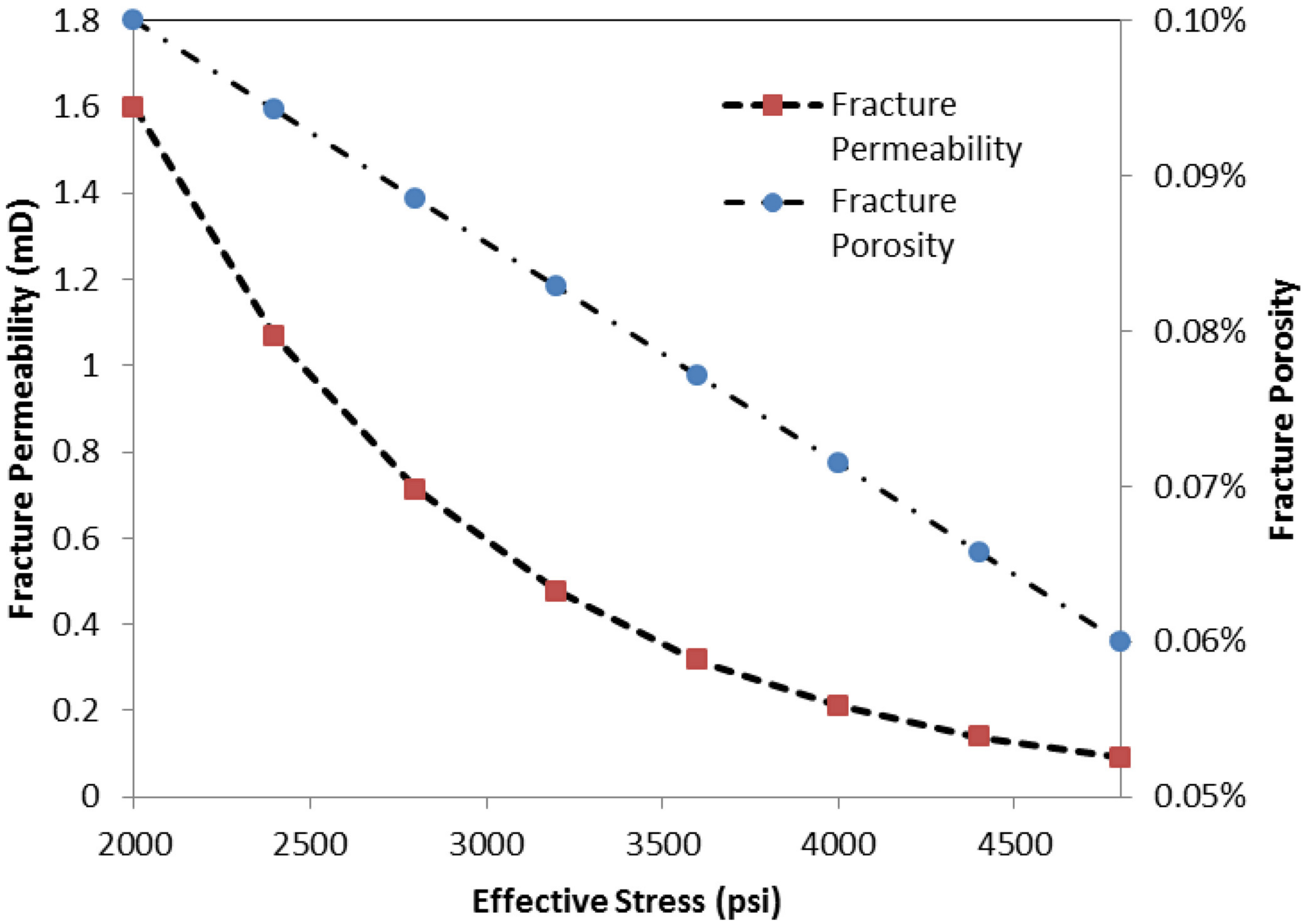

Figure 7—Porosity and permeability of natural facture with effective stress for natural fractures

4. Substitute the modified porosity and permeability values in calculation of the accumulation term and flow term for the next iteration.

Stress-sensitive fracture reservoir simulation and analysis

As shown in Figure 6, a multi-stage hydraulic fractured horizontal well in an extremely tight, uniformly porous and/or fractured reservoirs is considered in this study. The complicated fracture system, which includes hydraulic fracture and natural fractures, is assumed to exist only inside SRV. Fluids in this reservoir are water and gas. However, the water saturation is set at residual values as an immobile phase. Thus this is actually a single-phase gas flow problem and is modeled by the two phase flow reservoir simulator. The properties for the fractures, matrix, and fluids are given in Table 1.

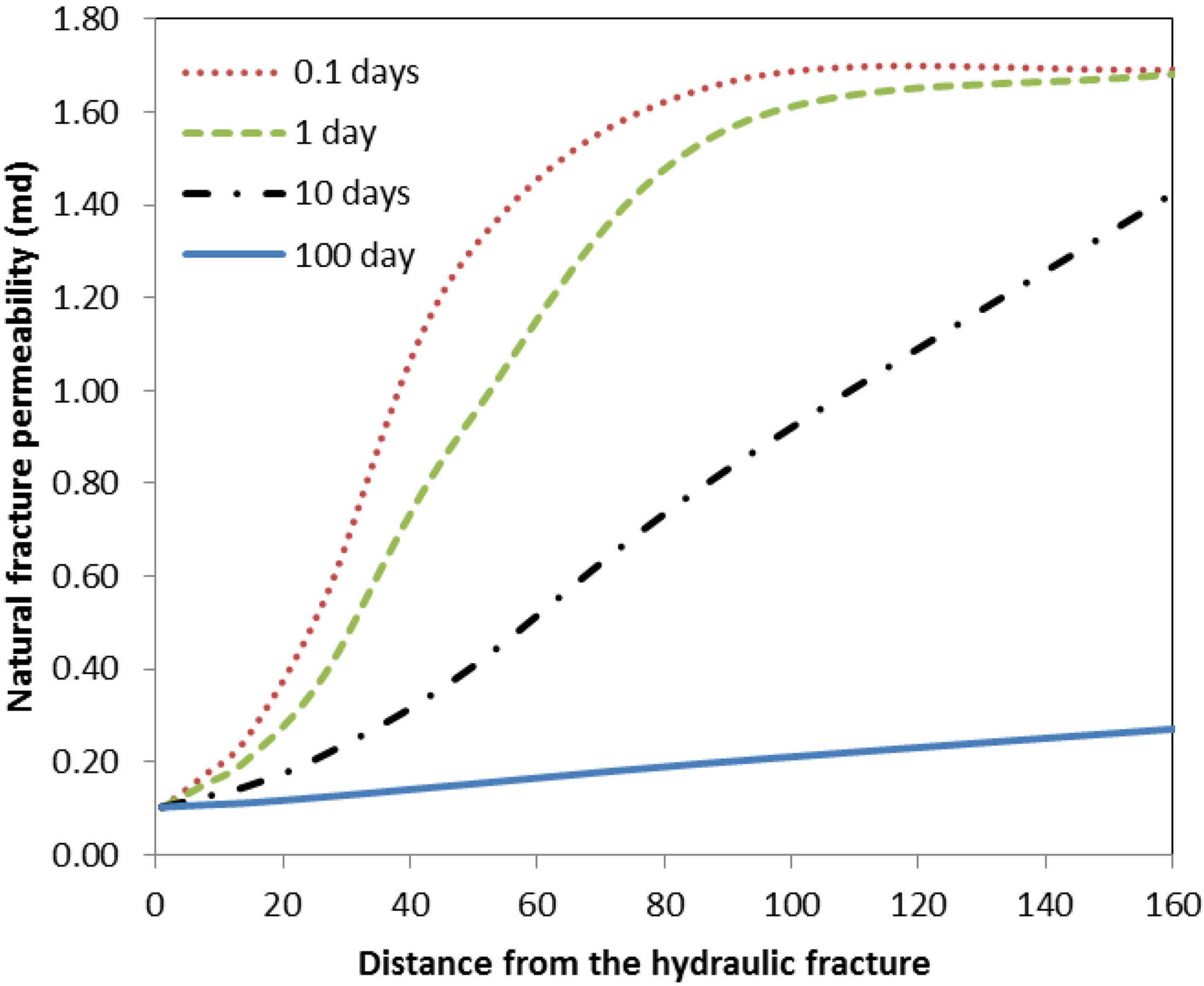

Figure 8—Simulated natural fracture permeability change with time and space

In this case, the formation is over-pressured with a pressure gradient of0.65psi/ft initially. The initial pressure for the whole reservoir is 5,800psi and well is produced with a constant pressure of 1,000psi. The stress is assumed to be isotropic and has a depth gradient corresponding to the acceleration of gravity multiplied by the rock density (1.0psi/ft). The initial porosity and permeability are obtained using the initial pressure and stress field and the correlation is shown in Equation 10 and Figure 7. (k_0 = 12.5md and C = 0.001). Hydraulic fracture conductivity in this study is assumed to be infinite, which can be achieved by merging well grids and hydraulic fracture grids numerically.

To reduce the calculation time, only one hydraulic fracture with its associated SRV and single porosity area is simulated with the following two considerations. The matrix permeability outside SRV is so small that blocks the flow interference between two nearby hydraulic fractures. Besides, we assume properties of these twenty fracture-associated areas are similar. Twenty times of the simulated production will be the total production for this case with horizontal wells and 20 hydraulic fractures

Figure 8 shows the change of natural fracture permeability corresponding to different time and location. The X axis is the distance from the interested point to the hydraulic fracture planar. Initial fracture permeability is about 1.60md. The natural fracture permeability near the hydraulic fracture decreases rapidly once production begins from 1.6md to 0.1md in 0.1 days. It implies that the fluids inside these

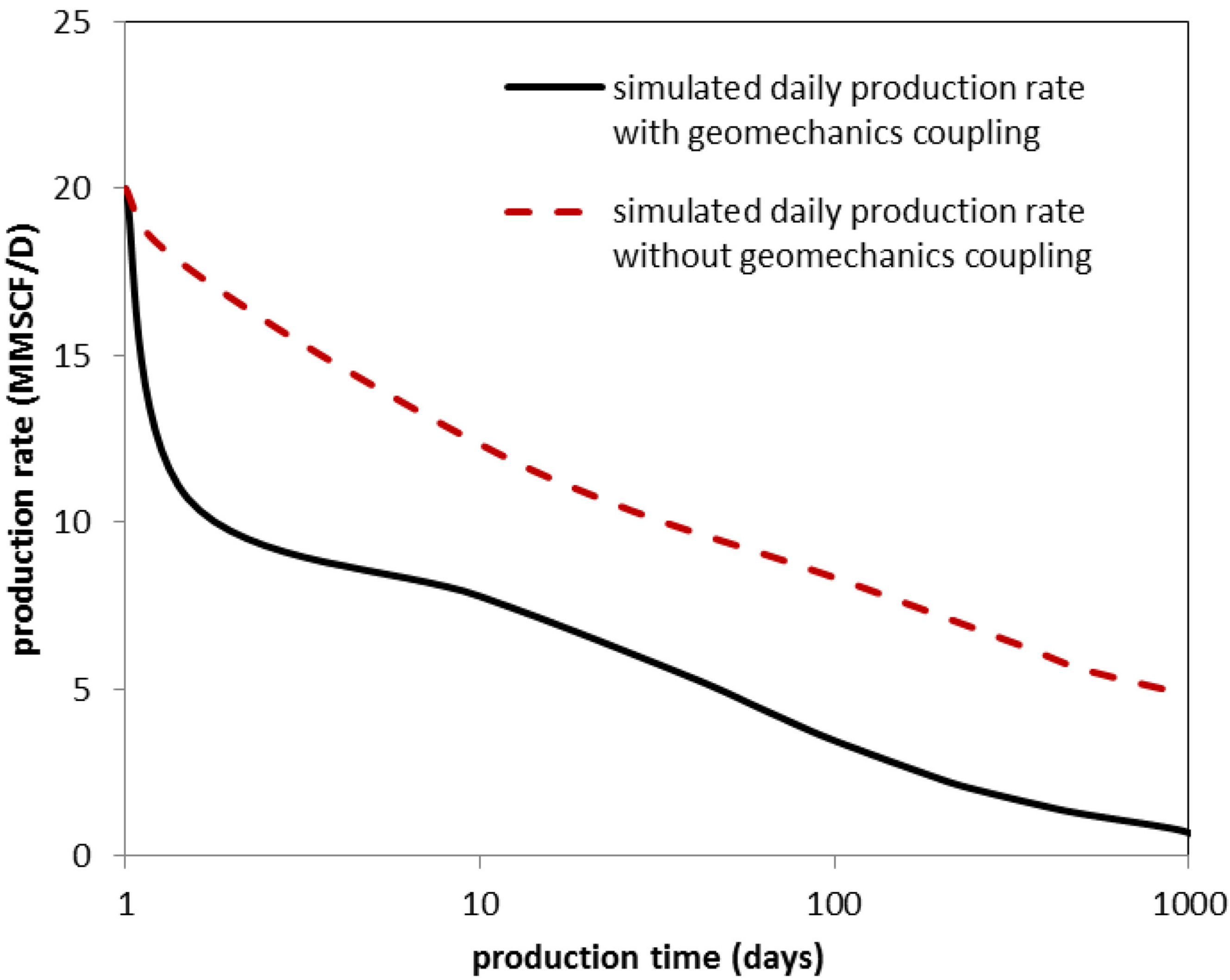

Figure 9—Production rate comparison between considering geomechanics coupling and not considering

natural fractures transport away quickly to the wellbore through hydraulic fractures. In the meanwhile, there are not enough fluids coming from nearby matrix and natural fractures to support and maintain the pressure. The decrease of permeability has a direct influence on the simulated production rate profile, which will be discussed in detail in the next figure. With the production going on, fractures farther away from the hydraulic fracture planar begin to be influenced. On the 10th day, the geomechanical influence extends to the whole interested area. On the 100th day, fracture permeability in this whole area is very low with an average value around 0.15md.

Figure 9 compares the production rate profiles of two simulation cases. The first one considers the geomechanical coupling effect on fluid flow simulation and the second one without geomechanical effect. All the input parameters keep the same as listed in Table 1. Both of these two curves start at the same production rate of 20MMSCF/day and then decline with time. The decline rate of first case (80% in first 100 days) is sharper than the second one (50% in first 100 days). The variation in production rate always exists from the early production phase to the late production phase.

A comparison of production rate decline curve considering the difference of wellbore pressure is shown in Figure 10. One well is produced with constant bottomhole pressure of 1,000psi and the other 2,400psi. The initial production rate for the 2,400psi case is lower but its decline rate is also lower than the other

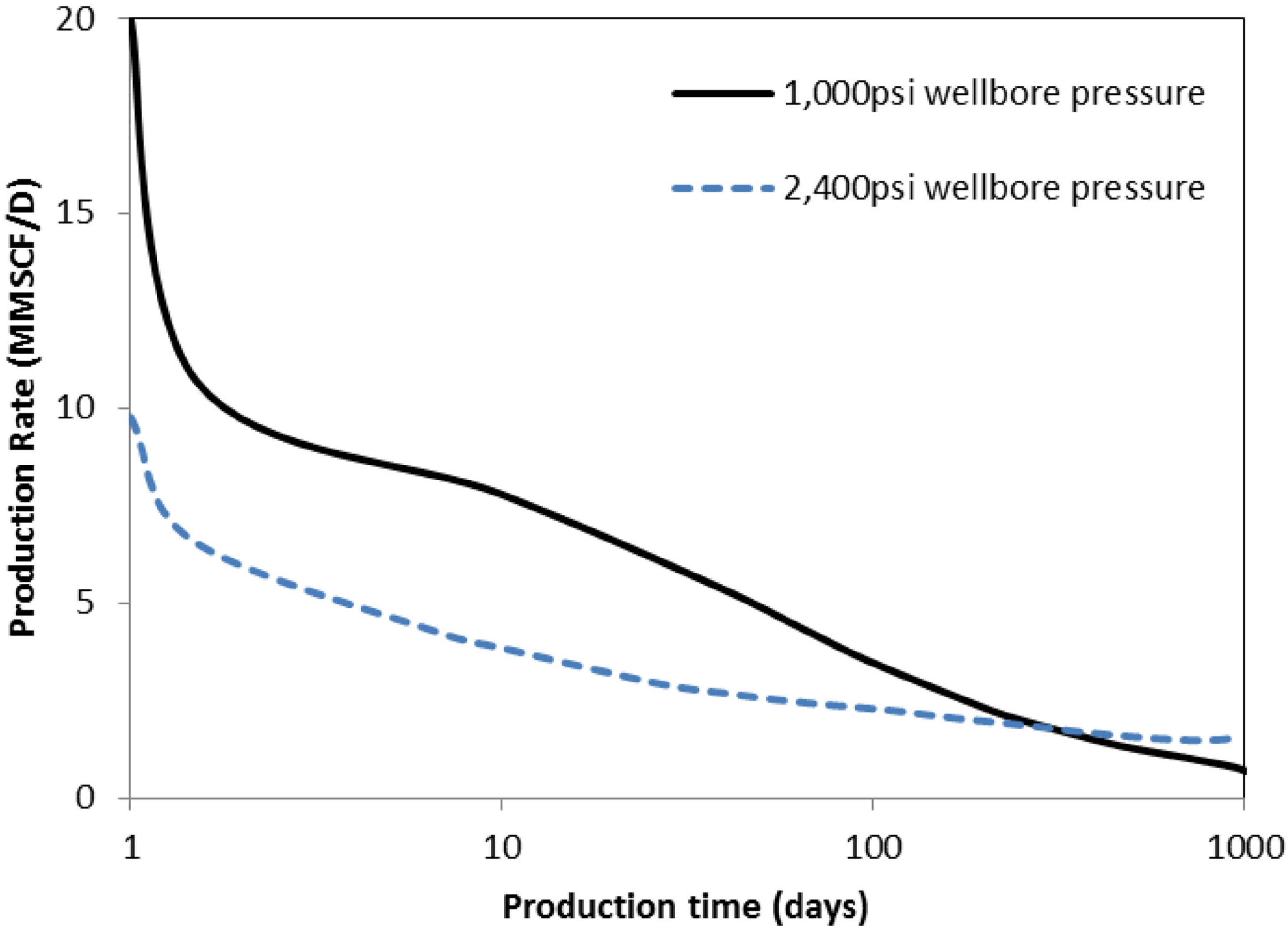

Figure 10—Comparison of production rate decline curve considering the difference of wellbore pressure

one. Its production rate exceeds the 1,000psi production well after 1 year. It indicates that the restricted rate well might have higher cumulative gas production.

Summary

This paper discusses a fully coupled geomechanics and fluid flow model to accurately simulate the field of stress and fluid flow in shale gas reservoirs. We describe the mathematical formulation and numerical method for fluid flow and geomechanics in a multi-porosity medium. Empirical relationships between fracture closure and applied stress (isotropic stress conditions and shear dilation) are incorporated, based on the literature where testing was completed under laboratory conditions. Therefore the stress dependency of shale natural fractures is quantified and modeled in its full complexity. The natural fractures in this model are characterized as stiff, self-propped, and prone to closure. It represents an extension of our earlier “hybrid-fracture model” (DFN for the hydraulic fractures, MINC for natural fractured area inside SRV, and single porosity for the area outside SRV) that did not account for stress-dependent fracture properties

As application examples, we run several simulations. First we compared the simulation results of two cases: one considers the geomechanical coupling effect on fluids flow and the other not. We also calculated the simulated fracture permeability change with time for the first case. Our simulation indicates that the closing of natural fractures, due to the change in subsurface stress induced by production, is one of the main mechanisms for a high decline rate observed in the early phase of shale gas production data.

We simulated the production rate profile in a stress-sensitive fractured reservoir with two different production pressures. It indicates the restricted rate well might have a higher cumulative gas production in a long production period.

Acknowledgments

This work was supported in part by EMG Research Center and UNGI of Petroleum Engineering Department at Colorado School of Mines and by Foundation CMG.

Nomenclature

A	Interface area between grid blocks [ft^2]
D	Coefficient of molecular diffusion [ft^2/day]
F_b	Body force [lbf]
F	Mass flux per unit volume of reservoir [lbmol/ft^3/day]
f	Fugacity of component in oil or gas phase [psi]
G	Shear modulus [psi]
K	Equilibrium ratio of component [-]
k	Absolute permeability [md]
k_r	Relative permeability of phases [-]
N	Mass accumulation per unit volume of reservoir [lbmol/ft^3]
n_c	Total number of hydrocarbon components [-]
n_b	Total number of grid blocks [-]
$\tilde{n}$	Mole fraction of oil or gas phase over whole hydrocarbon system [-]
P	Reservoir pressure [psi]
P_c	Capillary pressure [psi]
P_σ	Parachor value [-]
q	Sink/source per unit volume of reservoir [lbmol/ft^3/day]
R	Ideal gas constant [$ft^3psiR^{-1}lbmol^{-1}$]
S	Saturation of water, oil or gas phase [-]
T	Temperature [°F]
t	Time [days]
u	Displacement [ft]
V	Volume [ft^3]
$\vec{v}$	Darcy velocity of water, oil or gas phase [ft/day]
x	Molar fraction in oil phase [-]
y	Molar fraction in gas phase [-]
Z	Compressibility factor [-]
z	Total molar fraction in hydrocarbon system of component [-]
α	Biot coefficient [-]
β	Linear thermal expansion coefficient [R^{-1}]
Φ	Fugacity coefficient [-]
ϕ	Reservoir porosity [-]
σ	Stress [psi]
ρ	Molar density of water, oil or gas phase [lbmol/ft^3]
μ	Viscosity [cP]
μ	Chemical potential [psi]
ε_v	Volumetric strain [-]
λ	Lames constant [psi]

v Poisson's ratio [-]
ψ Flow potential [psi]
η A set of neighboring grid blocks of a grid block [-]

Subscripts

g Gas phase
i Index of mass component
k Index of primary variables
m Mean stress
n Index of grid block
$nm+1/2$ A proper averaging at the interface between grid blocks *n* and *m*
o Oil phase
p Iteration level
w Water phase
β Fluid phase
κ Index of primary equations
0 Reference state

References

Apaydin, Osman. *New Coupling Considerations Between Matrix and Multiscale Natural Fractures in Unconventional Resource Reservoirs*. Diss. Colorado School of Mines, 2012.

Baghbanan, Alireza, and Lanru Jing. "Stress effects on permeability in a fractured rock mass with correlated fracture length and aperture." *International Journal of Rock Mechanics and Mining Sciences* **45.8** (2008): 1320–1334.

Bustin, R.M., A.M.M. Bustin, X. Cui, D.J K Ross, and V.S. Murthy Pathi, 2008, "Impact of Shale Properties on Pore Structure and Storage Characteristics," SPE 119892, presented at the SPE Gas Production Conference, 16-18 November, Fort Worth, Texas.

Cipolla, C.L., N.R. Warpinski, M.J. Mayerhofer, E.P. Lolon, and M.C. Vincent, 2009, "The Relationship Between Fracture Complexity, Reservoir Properties, and Fracture Treatment Design," SPE 115769 presented at the SPE ATC&E, Denver, Colorado, U.S.A.

Davies, J. P., and D. K. Davies. "Stress-dependent permeability: characterization and modeling." *SPE Journal* **6.02** (2001): 224–235.

Gutierrez, M., L. E. Øino, and R. Nygård. "Stress-dependent permeability of a de-mineralised fracture in shale." *Marine and Petroleum Geology* **17.8** (2000): 895–907.

Jaeger, John Conrad, Neville GW Cook, and Robert Zimmerman. *Fundamentals of rock mechanics*. John Wiley & Sons, 2009.

Miller, Randall S., Michael Conway, and Greg Salter. "Pressure-Dependant Permeability in Shale Reservoirs Implications for Estimated Ultimate Recovery." Paper AAPG Search and Discovery 90122VC 2011 presented at the AAPG Hedberg Conference, Austin, Texas. 2010.

Meissner, Fred F. "*Petroleum geology of the Bakken Formation Williston basin, North Dakota and Montana*." (1978): 207–227.

Rutqvist, J., Wu, Y. S., Tsang, C. F., & Bodvarsson, G. (2002). A modeling approach for analysis of coupled multiphase fluid flow, heat transfer, and deformation in fractured porous rock. *International Journal of Rock Mechanics and Mining Sciences,* **39**(4), 429–442.

Settari, Antonin, and Dale A. Walters. "Advances in coupled geomechanical and reservoir modeling with applications to reservoir compaction." *Spe Journal* **6.03** (2001): 334–342.

Settari, A. "Reservoir compaction." *Journal of petroleum technology* **54.08** (2002): 62–69.

Soeder, D.J., 1988, “Porosity and Permeability of Eastern Devonian Gas Shale,” *SPE Formation Evaluation,* pp. 116–124.

Winterfeld P. H. and Wu Y.-S.: Simulation of CO2 sequestration in brine aquifers with geomechanical coupling, in *Computational Models for CO2 Sequestration and Compressed Air Energy Storage,* chapter 8, edited by J. Bundschuh and R. Al-Khoury, CRC Press, 2014.

Wang, Cong, Ding, Didier Yu and Yu-Shu Wu. “Characterizing Hydraulic Fractures in Shale Gas Reservoirs Using Transient Pressure Tests.” SPE Hydraulic Fracturing Technology Conference. Society of Petroleum Engineers, 2013.

Wang, C., & Wu, Y.-S. (2014, April 1). Modeling Analysis of Transient Pressure and Flow Behavior at Horizontal Wells with Multi-Stage Hydraulic Fractures in Shale Gas Reservoirs. *Society of Petroleum Engineers*. doi: 10.2118/168966-MS

Wang, F.P., R.M. Reed, J.A. Jackson, and K.G. Jackson, 2009. “Pore Networks and Fluid Flow in Gas Shales,” SPE 124253, presented at the 2009 SPE Annual Technical Conference and Exhibition held in New Orleans, Louisiana, USA, 4–7 October.

Wu, Yu-Shu, and Perapon Fakcharoenphol. “A unified mathematical model for unconventional reservoir simulation.” SPE-142884, presented at the SPE EUROPEC Conference, 2011.

Wu, Y. S., Li, J., Ding, D., Wang, C., & Di, Y. A Generalized Framework Model for the Simulation of Gas Production in Unconventional Gas Reservoirs. *SPE Journal,* 2014

Xiong, Y., Winterfield, P. H., Wu, Y.-S., & Huang, Z. (2014, August 28). Coupled Geomechanics and Pore Confinement Effects for Modeling Unconventional Shale Reservoirs. *Society of Petroleum Engineers*. doi: 10.15530/urtec-2014-1923960

Xiong, Y., Fakcharoenphol, P., Winterfeld, P., Zhang, R., & Wu, Y.-S. (2013, September 16). Coupled Geomechanical and Reactive Geochemical Model for Fluid and Heat Flow: Application for Enhanced Geothermal Reservoir. *Society of Petroleum Engineers*. doi: 10.2118/165982-MS

Zhang, J., et alet al. “Stress-dependent fluid flow and permeability in fractured media: from lab experiments to engineering applications.” *Rock Mechanics and Rock Engineering 40.1* (2007): 3–21.